Tomographic diffractive microscopy with agile illuminations for imaging targets in a noisy background

T. Zhang,[1] C. Godavarthi,[1] P. C. Chaumet,[1] G. Maire,[1] H. Giovannini,[1] A. Talneau,[2] C. Prada,[3] A. Sentenac,[1,*] and K. Belkebir[1]

[1]Aix Marseille Université, CNRS, Centrale Marseille, Institut Fresnel, UMR 7249, 13013 Marseille, France

[2]Laboratory for Photonics and Nanostructure, 91460 Marcoussis, France

[3]Institut Langevin, CNRS, ESPCI ParisTech, PSL Research University, 1 rue Jussieu, F-75005 Paris, France

*Corresponding author: anne.sentenac@fresnel.fr

Received September 24, 2014; revised January 5, 2015; accepted January 5, 2015; posted January 7, 2015 (Doc. ID 223667); published February 10, 2015

Tomographic diffractive microscopy is a marker-free optical digital imaging technique in which three-dimensional samples are reconstructed from a set of holograms recorded under different angles of incidence. We show experimentally that, by processing the holograms with singular value decomposition, it is possible to image objects in a noisy background that are invisible with classical wide-field microscopy and conventional tomographic reconstruction procedure. The targets can be further characterized with a selective quantitative inversion. © 2015 Optical Society of America

OCIS codes: (100.3010) Image reconstruction techniques; (110.3175) Interferometric imaging.
http://dx.doi.org/10.1364/OL.40.000573

Detecting and characterizing targets in a noisy environment is a major challenge of current imaging tools due to its wide domain of applications from radar-imaging of targets in natural soil to optical imaging of organelles in cells. It has stirred a wealth of research essentially in the acoustic and electromagnetic domains [1–3] where the absence of any analogical imager has fostered the development of numerical treatments for processing the data into a readable image. A tool of choice for extracting the target signature from a noisy environment is the time-reversal technique or its monochromatic counterpart, the DORT procedure (for the French acronym décomposition de l'opérateur de retournement temporel, Time Reversal Operator Decomposition). This procedure requires to record the field (amplitude and phase) scattered by the sample for various illuminations in order to build the scattering matrix $\mathbf{K}$ of the target ($\mathbf{K}$ relies the incoming field to the outgoing one) on which a singular value decomposition (SVD) is performed. It can be shown that for point-like scatterers in the single scattering regime, a few singular vectors of $\mathbf{K}$ (or equivalently, the eigenvectors of the time reversal operator $\mathbf{K}^{\dagger}\mathbf{K}$ where † denotes the conjugate transpose), hereafter called the DORT vectors, correspond to incident fields that focus selectively on the targets. This efficient approach has been widely documented in sonar or radar imaging and it has been recently applied to the optical domain [4] for focusing on gold nanoparticles placed under an aberrating layer.

The DORT or time-reversal technique permits to generate agile incident fields that focus on targets embedded in a randomly inhomogeneous medium, but it does not provide images of the sample [4]. To localize and characterize quantitatively the targets (for example estimating their size and permittivity), additional data processing is required [3,5]. Recently, it was proposed to apply an inversion procedure on data obtained with DORT illuminations [3,6]. It was shown on synthetic experiments that this combined DORT-inversion approach was significantly better than standard inversion techniques for estimating targets buried in an inhomogeneous soil. Indeed, the DORT illuminations dimmed the influence of the clutter and allowed the restriction of the investigation domain to small regions surrounding the targets [6]. In this work, we adapt this procedure to optical microscopy and show experimentally its interest for imaging objects of various sizes in a noisy background.

Presently, the most powerful optical microscopy technique yielding three-dimensional images of marker-free samples is tomographic diffraction microscopy (TDM) also known as synthetic aperture microscopy or diffraction phase microscopy [7–15]. In this approach, the sample is illuminated with a collimated beam under various incident angles and polarization states, and its scattered field (phase and amplitude) is recorded for a large number of observation directions within the numerical aperture (NA) of the microscope objective. The sample is usually reconstructed from the far-field data with linear inversion techniques (based on Fourier transforms), albeit more sophisticated inversion methods have been reported [15]. The interest of TDM is that it provides directly the scattering matrix of the sample, and it is thus perfectly adapted to the implementation of the DORT-inversion procedure.

The TDM developed in this work is based on a reflection microscope in which an off-axis holography technique and polarizers have been introduced to recover the phase, amplitude, and polarization of the field at the image plane [14,16,17], see Fig. 1(a). A collimated beam (with $\lambda = 632.8$ nm), controlled angularly by a fast steering mirror (Newport FSM-300), with its polarization state adjusted by the half-wave plate HW_1, illuminates the sample through an air objective with NA = 0.95 (Zeiss Epiplan-Apochromat ×50). For each direction of incidence $\mathbf{q}_{l=1,\ldots,L}$, two independent linear incident polarization states of the beam are considered, $\hat{\mathbf{s}}(\mathbf{q}_l) = \mathbf{q}_l \times \hat{\mathbf{z}}$ or

$\hat{\mathbf{p}}(\mathbf{q}_l) = \mathbf{q}_l \times \hat{\mathbf{s}}(\mathbf{q}_l)$, yielding a total number of $2L$ illuminations. The vectorial field scattered by the sample is recorded at the image plane of the microscope objective on a sCMOS camera (with a pixel size about 30 nm after magnification) (Andor Zyla 5.5) after interference with a reference beam whose polarization state is monitored by the half-wave plate HW_2. All measurements are normalized by adjusting the experimental amplitude of the reflected specular beam to the theoretical reflection coefficient of the planar substrate on which the sample is deposited [17]. After some straightforward manipulations, the recorded data is cast into a $2L \times 2M$ scattering matrix $\mathbf{K}$ whose complex coefficients $K^{\hat{\mathbf{a}},\hat{\mathbf{b}}}_{m,l}$ represents the a-polarized component of the field diffracted by the sample along the diffracted direction $\mathbf{k}_{m=1,\ldots,M}$ when the illumination is a b-polarized incident plane wave propagating along the $\mathbf{q}_{l=1,\ldots,L}$ directions, where $\hat{\mathbf{a}} = \hat{\mathbf{s}}(\mathbf{k}_m)$ or $\hat{\mathbf{p}}(\mathbf{k}_m)$ and $\hat{\mathbf{b}} = \hat{\mathbf{s}}(\mathbf{q}_l)$ or $\hat{\mathbf{p}}(\mathbf{q}_l)$.

The sample under study is made of four resin cylinders with permittivity 2, height 170 nm and radii 250, 200, 150, and 100 nm, deposited on a reflective silicon substrate, as shown in Fig. 1(b). For estimating such a thin sample with global transverse width about 7 wavelengths, $L = 5 \times 5$ directions of illumination and $M = 60 \times 60$ directions of observation regularly spaced within the NA of the objective have been taken. The number of observation points ensures that the scattered field is correctly sampled, while the number of illuminations ensures an appropriate data over unknown ratio in the reconstruction process as will be shown below.

To image the sample, we first generate a conventional bright field image by summing over all the illuminations the experimental intensity of the field recorded at the microscope image plane, see Fig. 2(a). Four cylinders with various widths are visible as expected. Then, we calculate the SVD of the scattering matrix $\mathbf{K}$ [18], $\mathbf{K} = \Sigma_{j=1}^{2L} \mathbf{v}_j \sigma_j \mathbf{u}_j^{\dagger}$, where σ_j is the singular value of $\mathbf{K}$, which is real and non-negative. In this expression, the $2M$ vector $\mathbf{v}_j$ gives the vectorial field diffracted by the sample when the illumination is a sum of plane waves with directions $\mathbf{q}_{l=1\ldots L}$ with $\hat{\mathbf{p}}$ and $\hat{\mathbf{s}}$ amplitudes fixed by the $2L$

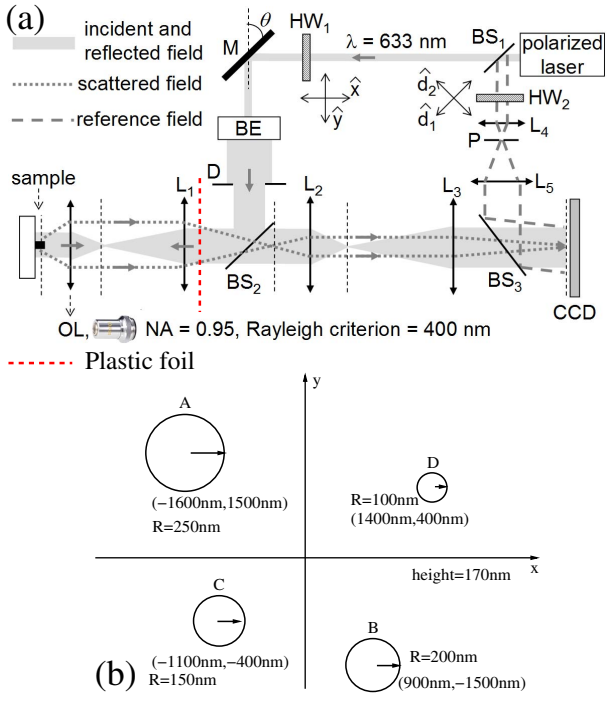

Fig. 1. (a) Schematic of the full-polarized TDM setup: M, rotative mirror. BE, beam expander; D, diaphragm; BS, beam splitter; OL, objective lens; P, pinhole; L_1, tube lens; L_2 and L_3, relay lenses ($f' = 3.5$ and 20 cm, respectively). HW_1 and HW_2 are the half-wave plates on the incident field and reference field, respectively. Red dashed line, plastic aberrating layer. (b) Sample geometry in the transverse cut plane. It is composed of four resin cylinders with permittivity 2, height 170 nm, and different radii deposited on a silicon substrate with permittivity $15.07 + 0.148i$ at the illumination wavelength 632.8 nm.

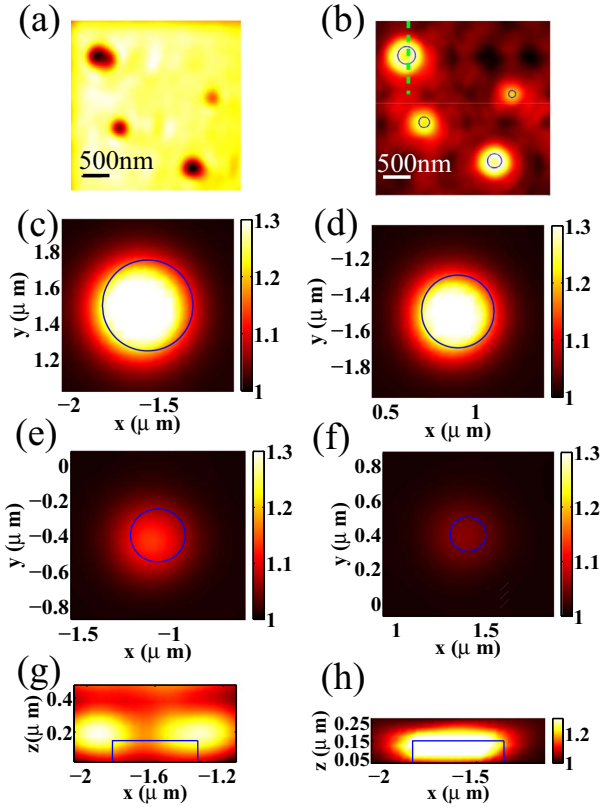

Fig. 2. Noise-free configuration (a) and (b) qualitative images of the sample in the (x, y) plane. (a) Bright-field conventional microscope image generated by summing the experimental intensity recorded at the image plane of the TDM for the $2L = 50$ illuminations. (b) DORT image obtained by summing the intensities of the fields generated by all the singular vectors $\mathbf{v}_{j=1,\cdots,2L}$ of the scattering matrix at $z = 100$ nm above the substrate. (c)–(f) Selective quantitative reconstructions of the four cylinders. The quantitative inversion procedure is run on the scattered fields $\mathbf{u}_{j=1\ldots 2L}$ obtained for the agile illuminations $\mathbf{v}_{j=1\ldots 2L}$. The investigation domain is restricted to a $2 \times 2 \times 0.25$ μm^3 box surrounding one scatterer at a time. The reconstructed permittivity map is displayed in the (x, y) plane at $z = 100$ nm. (g)–(h) Image of the sample in the (x, z) plane along the line passing through the middle of the largest cylinder indicated in subplot (b). (g) qualitative DORT image [as in subplot (b)]. The bright tore observed above the cylinder reflects the complexity of the DORT-focusing behavior when the scatterer size is comparable to the wavelength. (h) Selective quantitative reconstruction of the largest cylinder. The scatterer shape is significantly improved compared to (g).

vector $\mathbf{u}_j$. Due to the reciprocity theorem, the $2L$ vector $\mathbf{u}_j$ can also be interpreted as the vectorial field diffracted along the $-\mathbf{q}_{l=1\ldots L}$ direction when the illumination is a sum of plane waves with directions $-\mathbf{k}_{m=1\ldots M}$ and $\hat{\mathbf{p}}$ and $\hat{\mathbf{s}}$ amplitudes fixed by the $2M$ vector $\mathbf{v}_j$. For forming the DORT agile illuminations, it is preferable to consider the reciprocal configuration, as the beam given by $\mathbf{v}_j$ contains many more plane wave directions than that given by $\mathbf{u}_j$.

To get an insight on the focusing property of $\mathbf{v}_{j=1,\ldots,2L}$ beams, its field $\mathbf{E}_j^{\mathrm{SV}}(\mathbf{r})$ in the sample domain is generated by propagating each plane wave component in a simplified medium made of a bare air-silicon interface. One gets

$$\mathbf{E}_j^{\mathrm{SV}}(\mathbf{r}) = \sum_{m=1}^{M} v_j^p(m)\mathbf{E}^p(\mathbf{r}, -\mathbf{k}_m) + v_j^s(m)\mathbf{E}^s(\mathbf{r}, -\mathbf{k}_m), \quad (1)$$

where $\mathbf{E}^{p(s)}(\mathbf{r}, -\mathbf{k}_m)$ is the field at $\mathbf{r}$ obtained when the silicon interface is illuminated by a $p(s)$-polarized plane wave with direction $-\mathbf{k}_m$, and $v_j^{p(s)}(m)$ is the $p(s)$-polarized component of $\mathbf{v}_j$ for the mth direction. This simulation is only a crude approximation of the actual field induced by $\mathbf{v}_j$ in the sample domain, as it does not account for the cylinder's influence. We observed (not shown) that the field intensity of all the singular vectors presented bright patterns about the cylinders (which are related to the significant moments of the multipole expansion of the field radiated by each target [5]), and thus all the singular vectors bore useful information for the reconstruction process.

Figure 2(b) displays the sum of the intensities of the singular vectors backpropagated following Eq. (1) at $z = 100$ nm above the substrate. The four bright patterns that are visible over a null background demonstrate the focusing properties of these agile illuminations. Yet, the three-dimensional intensity distribution remains significantly different from that of simple focusing beams, see Fig. 2(g) as it reflects the complexity of the DORT vectors behavior when the scatterers size is comparable to the wavelength and the imaging configuration is not free-space. In particular, the rather small axial width of the focused fields is due to the interference between the incident plane waves and their reflection by the silicon substrate [19].

In a second step, we improve the sample characterization using an iterative inversion method [20] that takes advantage of the DORT focusing properties [6]. Instead of running the inversion procedure on the $2L \times 2M$ scattered field of the scattering matrix $\mathbf{K}$ that are obtained for the $2L$ plane waves illumination, we consider the $2L \times 2L$ scattered field given by $\mathbf{u}_{j=1,\ldots,2L}$ obtained for the $2L$ agile illuminations $\mathbf{v}_{j=1,\ldots,2L}$. Note that as long as all the singular vectors are kept in the reconstruction procedure, the DORT preprocessing corresponds to a simple rearrangement of the data and not to a data reduction technique. The diminution of the scattered field data is entirely compensated by the information carried out by the complex illumination patterns.

The inversion procedure is thoroughly described in Ref. [20]. Basically, it consists in building a series of sample permittivity contrast χ_n in a given investigation domain Ω so as to minimize iteratively the distance between all the measured scattered field components $\mathbf{u}_j(l)$, for $j = 1, \ldots, 2L$ and $l = 1, \ldots, L$, to the fields scattered by the nth estimation χ_n simulated in the same conditions. The investigation domain, estimated with the bright field image, is taken equal to $5\ \mu\mathrm{m} \times 5\ \mu\mathrm{m} \times 0.2\ \mu\mathrm{m}$ with a mesh size of 50 nm yielding a data over unknown ratio about two.

The DORT processing permits, thanks to its focusing properties, Figs. 2(b), the restriction of the investigation domain Ω to the most illuminated regions. As a result, the computation time required by the inversion is drastically reduced, and the reconstruction is more accurate. In our case, the sample is reconstructed by running the inversion process on a $2\ \mu\mathrm{m} \times 2\ \mu\mathrm{m} \times 0.25\ \mu\mathrm{m}$ investigation box centered about each target successively. Note that when the targets exhibit very different scattering power, a successive selective inversion is more efficient than a global reconstruction, even though the illumination focus on different targets simultaneously.

Figures 2 display the transverse cut of the permittivity map of each cylinder (c)–(f) and an axial cut of the permittivity of the biggest cylinder (h). We observe that the quantitative inversion ameliorates significantly the characterization of the targets as compared to the DORT image especially in the axial plane, compare Figs. 2(g) and 2(h). The reconstructions are in satisfactory agreement with the actual permittivity profile and the expected resolution about $\lambda/4$ NA ≈ 167 nm [14,15]. The permittivity underestimation (especially for the smallest cylinder) is linked to the overestimation of the transverse footprint due to the limited resolution.

We now consider the much more difficult configuration in which the sample is placed behind an aberrating layer. To this aim, a piece of plastic foil is placed through the illumination and collection paths in the experiment, see Fig. 1(a). In this noisy configuration, the conventional bright field microscopy image of the sample is so deteriorated that solely the largest cylinder is visible, see Fig. 3(a). On the other hand, the DORT focusing image obtained by summing all the $\mathbf{v}_{j=1,\ldots,2L}$ field intensities in the sample domain calculated with Eq. (1) (thus neglecting the influence of the aberrating layer and of the cylinders) permits to distinguish the four cylinders, see Fig. 3(b). The relative size of the targets can even be roughly guessed, and the axial width of the focused beams is similar to that obtained in the noiseless configuration about one half of the wavelength Fig. 3(g). Note that the multiple scattering between the cylinders and the aberrating layer is negligible in this experiment. Hence, the image of the smallest scatterer in this linear regime gives a good approximation of the resolution one can expect with this noise level.

The selective inversion procedure ameliorates further the characterization of the cylinders by retrieving their round shape and axial dimensions, see Figs. 3(c)–3(f), and 3(h), albeit with a significant underestimation of the permittivity. Note that, in this noisy configuration, the inversion procedure applied to the data without the DORT preprocessing failed in retrieving the two smallest cylinders.

In conclusion, TDM is usually performed with plane wave illuminations that are not always the appropriate

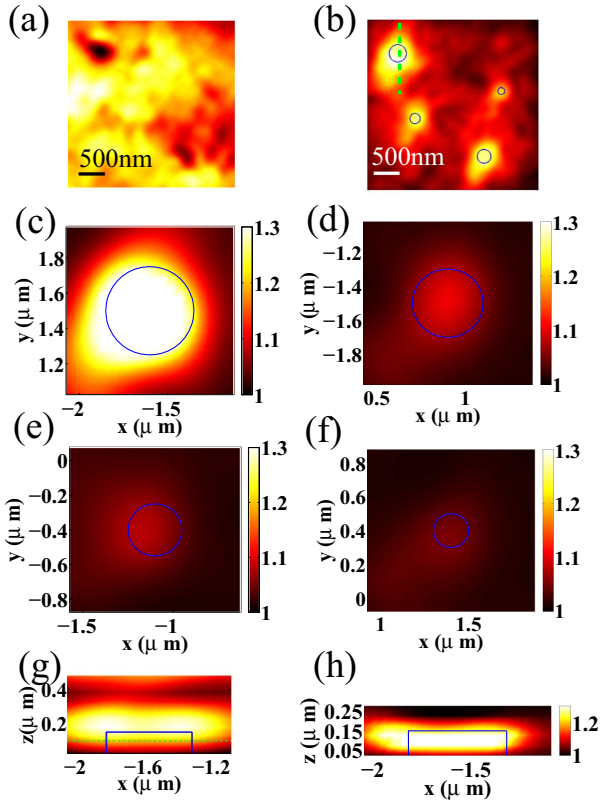

Fig. 3. Same as Fig. 2 but in the noisy configuration.

basis for probing the sample, especially when the latter is made of isolated small scatterers. Rearranging the data so that the illuminations correspond to the singular vectors of the scattering matrix (or DORT vectors) permits to enhance significantly the signal-to-noise ratio. The simple numerical backpropagation of the singular DORT vectors into the sample domain yields an accurate qualitative estimation of the sample that can be further ameliorated with a quantitative inversion technique. The hybrid DORT-inversion approach was shown to be able to distinguish cylinders of various radii in a noisy configuration that were invisible on a conventional bright field microscopy image or with classical tomographic reconstruction techniques.

References and Note

1. C. Prada and M. Fink, Wave Motion **20**, 151 (1994).
2. H. Tortel, G. Micolau, and M. Saillard, J. Electromag. Waves Appl. **13**, 687 (1999).
3. A. Dubois, K. Belkebir, and M. Saillard, Inverse Probl. **20**, S63 (2004).
4. S. M. Popoff, A. Aubry, G. Lerosey, M. Fink, A. C. Boccara, and S. Gigan, Phys. Rev. Lett. **107**, 263901 (2011).
5. G. Micolau and M. Saillard, Radio Sci. **38**, 1038 (2003).
6. T. Zhang, P. C. Chaumet, E. Mudry, A. Sentenac, and K. Belkebir, Inverse Probl. **28**, 125008 (2012).
7. V. Lauer, J. Microsc. **205**, 165 (2002).
8. M. Debailleul, V. Georges, B. Simon, A. Beghin, R. Morin, and O. Haeberlé, Opt. Lett. **34**, 79 (2009).
9. B. Simon, M. Debailleul, A. Beghin, Y. Tourneur, and O. Haeberlé, J. Biophoton. **3**, 462 (2010).
10. Y. Cotte, F. Toy, P. Jourdain, N. Pavillon, D. Boss, P. Magistretti, P. Marquet, and C. Depeursinge, Nat. Photonics **7**, 113 (2013).
11. O. Haeberlé, K. Belkebir, H. Giovaninni, and A. Sentenac, J. Mod. Opt. **57**, 686 (2010).
12. E. Wolf, Opt. Commun. **1**, 153 (1969).
13. S. Kawata, O. Nakamura, T. Noda, H. Ooki, K. Ogino, Y. Kuroiwa, and S. Minami, Appl. Opt. **29**, 3805 (1990).
14. T. Zhang, Y. Ruan, G. Maire, D. Sentenac, A. Talneau, K. Belkebir, P. C. Chaumet, and A. Sentenac, Phys. Rev. Lett. **111**, 243904 (2013).
15. G. Maire, F. Drsek, J. Girard, H. Giovannini, A. Talneau, D. Konan, K. Belkebir, P. C. Chaumet, and A. Sentenac, Phys. Rev. Lett. **102**, 213905 (2009).
16. The experiment was automatized using the free soft-ware OpticsBenchUI.
17. G. Maire, Y. Ruan, T. Zhang, P. C. Chaumet, H. Giovannini, D. Sentenac, A. Talneau, K. Belkebir, and A. Sentenac, J. Opt. Soc. Am. A **30**, 2133 (2013).
18. M. Davy, T. Lepetit, J. de Rosny, C. Prada, and M. Fink, Prog. Electromagn. Res. **110**, 353 (2010).
19. E. Mudry, E. L. Moal, P. Ferrand, P. C. Chaumet, and A. Sentenac, Phys. Rev. Lett. **105**, 203903 (2010).
20. E. Mudry, P. C. Chaumet, K. Belkebir, and A. Sentenac, Inverse Probl. **28**, 065007 (2012).